Solar-Driven Water Splitting
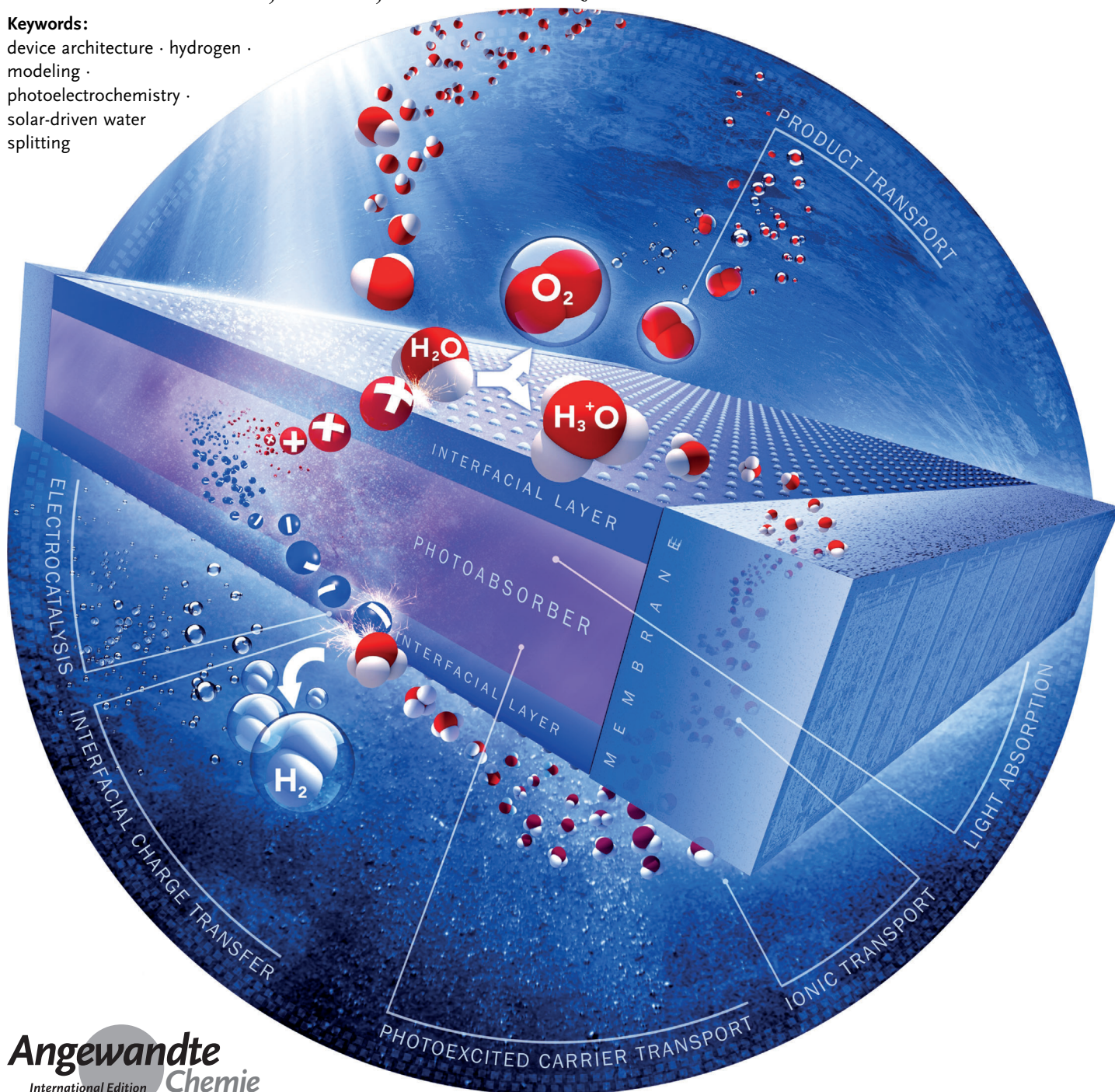
Modeling, Simulation, and Implementation of Solar-Driven Water-Splitting Devices

Chengxiang Xiang,* Adam Z. Weber,* Shane Ardo, Alan Berger, YiKai Chen, Robert Coridan, Katherine T. Fountaine, Sophia Haussener, Shu Hu, Rui Liu, Nathan S. Lewis, Miguel A. Modestino, Matthew M. Shaner, Meenesh R. Singh, John C. Stevens, Ke Sun, and Karl Walczak

Angewandte
International Edition
Chemie

▮▮▮▮ **Wiley Online Library**
↖↗

© 2016 Wiley-VCH Verlag GmbH & Co. KGaA, Weinheim

Angew. Chem. Int. Ed. **2016**, *55*, 2 – 17

These are not the final page numbers!

*A*n integrated cell for the solar-driven splitting of water consists of multiple functional components and couples various photo-electrochemical (PEC) processes at different length and time scales. The overall solar-to-hydrogen (STH) conversion efficiency of such a system depends on the performance and materials properties of the individual components as well as on the component integration, overall device architecture, and system operating conditions. This Review focuses on the modeling- and simulation-guided development and implementation of solar-driven water-splitting prototypes from a holistic viewpoint that explores the various interplays between the components. The underlying physics and interactions at the cell level is are reviewed and discussed, followed by an overview of the use of the cell model to provide target properties of materials and guide the design of a range of traditional and unique device architectures.

From the Contents

components as well as on the system design. Over the past few years, significant advances have been made in the discovery and development of materials for individual components as well as in the design and implemen-

1. Introduction

One attractive approach to circumvent the intermittent nature of solar irradiation is to store large-scale solar-converted energy in the form of chemical bonds, that is, in an artificial photosynthetic process at an average efficiency that is significantly higher than that of most crops.[1] Significant challenges still exist for the capture, conversion, and storage of solar energy through artificial photosynthesis. Of all the solar-driven fuel-forming devices, a solar-driven water-splitting cell has the simplest fuel-forming chemical reaction, and has demonstrated the highest efficiency, stability, and scalability.[2] Two distinctive systems—a discrete system in which a photovoltaic unit is electrically connected in series with an electrolyzer unit (PV-E) and a monolithically integrated photoelectrolysis system (PEC)—have demonstrated efficient, unassisted solar-driven water splitting on a laboratory scale. The PV-E system offers a modular approach that allows for the optimization of individual components and reduces the incompatibility of the materials between the power-generating and water-electrolysis units. For example, Si PV minimodules and perovskite-based solar cells have been used recently in the PV-E design,[3] and numerous demonstrations of commercial PV modules connected to electrolyzers have been performed at various scales.[4] Recent techno-economic analyses suggest high levelized hydrogen costs in the PV-E system relative to hydrogen produced by steam reforming or grid electrolysis (electrolyzer units operating with grid electricity) because of the high balance-of-system cost and the low capacity factor of the system.[5] The integrated PEC system, however, leverages a simplistic design that could provide many potential advantages relative to a PV-E system and offers a unique flexibility of design for the balance of systems.[2b,5c,6]

An integrated, intrinsically safe, solar-driven water-splitting device is generally comprised of light absorbers, electrocatalysts, membrane separators, and an electrolyte solution in a given system geometry. The overall solar-to-hydrogen (STH) conversion efficiency of such a system depends on the performance and materials properties of all the individual

[*] Dr. C. Xiang, Y. Chen, Prof. S. Hu,[+] Dr. R. Liu, Prof. N. S. Lewis, Dr. M. M. Shaner, Dr. K. Sun
Joint Center for Artificial Photosynthesis
California Institute of Technology
Pasadena CA 91125 (USA)
E-mail: cxx@caltech.edu

Dr. A. Z. Weber, Prof. M. R. Singh,[#] Dr. J. C. Stevens, Dr. K. Walczak
Joint Center for Artificial Photosynthesis
Lawrence Berkeley National Laboratory
Berkeley, CA 94720 (USA)
E-mail: azweber@lbl.gov

Prof. S. Ardo
Department of Chemistry
and Department of Chemical Engineering and Materials Science
University of California Irvine (USA)

Dr. A. Berger
Air Products and Chemicals, Inc.
Allentown (USA)

Prof. R. Coridan
Department of Chemistry and Biochemistry
University of Arkansas (USA)

Dr. K. T. Fountaine
Nanophotonics and Plasmonics Laboratory
Northrop Grumman Aerospace Systems
Redondo Beach (USA)

Prof. S. Haussener
Laboratory of Renewable Energy Science and Engineering, EPFL
Lausanne (Schweiz)

Prof. N. S. Lewis, Dr. M. M. Shaner, Dr. K. Sun
Division of Chemistry and Chemical Engineering
210 Noyes Laboratory, 127-72
California Institute of Technology, Pasadena (USA)

Dr. M. A. Modestino
School of Engineering, EPFL, Lausanne (Schweiz)

[+] Current address:
Department of Chemical and Environmental Engineering
Yale University (USA)

[#] Current address:
Department of Chemical Engineering
University of Illinois at Chicago (USA)

[iD] The ORCID identification number(s) for the author(s) of this article can be found under http://dx.doi.org/10.1002/anie.201510463.
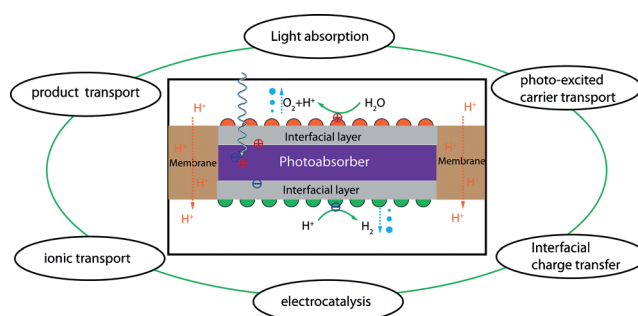
tation of solar-driven water-splitting devices at the system level. In the development of solar-driven water-splitting cells at the device level, multidimensional continuum modeling and simulation has played, and continues to play, a significant role in defining the target properties of the materials, predicting attainable device efficiencies,[7] constraining operating conditions,[8] providing cell dimensions,[9] comparing material and operating tradeoffs, and evaluating novel cell architectures and concepts.[10] Through the use of multiphysics modeling, one can understand operations and trade-offs at the device level and virtually integrate the components. Ideally, such modeling is coupled to the development of laboratory-scale devices, which have also progressed substantially over the last few years in terms of efficiency and stability.[2b, 3, 11]

The emphasis of solar-powered water splitting as a clean-energy-generation technology, and the recent emergence of simulation and prototype design as well as material integration in this field, makes a review of these topics timely. Although there has been a recent spate of reviews on the topic of solar fuels,[12] the focus of this one is unique in terms of examining the underlying multiphysics phenomena and design principles, including their implementation, from an integrated device point of view. This holistic perspective is necessary to move the field and technology closer towards commercialization; throughout, comments from this viewpoint will be made.

The Review is structured as follows. First, the range of coupled chemical and physical phenomena that occur in a PEC system across the various length scales will be described from the basis of a continuum-level model, namely, capture and transport of light in the semiconductor, electrocatalysis for the oxygen- and hydrogen-evolution reactions (OER and HER), ion transport in the membrane and aqueous electrolytes, transport of product gas, and coupled multicomponent interactions between these physicochemical phenomena. Next, simulation outputs and guidance will be explored in terms of different prototypical device systems, including unique ones that modeling has shown to be promising.

2. Continuum-Level Modeling

A functional solar-driven water-splitting cell integrates multiple (photo)electrochemical components that operate at

Figure 1. Schematic illustration of various coupled photoelectrochemical processes in an integrated solar-driven water-splitting cell.

different length and time scales. Figure 1 shows a schematic illustration of various photoelectrochemical processes in an integrated solar-driven water-splitting system. Key electrochemical processes include the absorption of light and transport of photoexcited charge in semiconductor materials, transport of interfacial charge and electrocatalysis for the HER and OER, transport of multicomponent ions in electrolytes, and transport of product gas. During steady-state operation of the cell, these processes are fully coupled together to produce a single rate of reaction for water splitting. As a result, modeling a single physical phenomenon or an individual component of a device does not provide sufficient insight into the behavior of an integrated device; a coupled multiphysics, multiscale model is required. For example, the physical phenomena governing the absorption and conversion of light into separated electronic charges within semiconductor materials operate at the nanometer scale, and alter the optimal morphology and structure of the photoelectrochemical assemblies at the micrometer scale, which ultimately influences the cell design and configuration at the centimeter or larger scale. This coupling is not just forward, as device configurations and operation constrain the selection of materials and operating points at the micrometer and nanometer scales.

A model that includes all the critical (photo)electrochemical processes in the integrated solar-driven water-splitting device can provide important principles to guide the discovery of materials, evaluate novel system designs, determine the operating conditions and constraints, and allow for a predictive, quantitative understanding of the system performance.

Chengxiang ("CX") Xiang is a Principle Investigator and Staff Scientist at the Joint Center for Artificial Photosynthesis (JCAP) at the California Institute of Technology. He received his PhD in Chemical and Material Physics at the University of California, Irvine in 2009 with Prof. E. M. Penner, and was a Postdoctoral Scholar for Prof. N. Lewis at the California Institute of Technology from 2009 to 2011. His research interests include the fabrication of solar-fuel prototypes, optoelectronic catalytic modeling of micro/nano-structured photoelectrochemical systems, and multi-ion transport modeling in solution and polymer electrolytes.

Adam Z. Weber received his BSc and MSc from Tufts University in 1999, and his PhD from the University of California, Berkeley in 2004 with J. Newman. He is now leader of the Energy Conversion Group and thrust coordinator at the Joint Center for Artificial Photosynthesis at Lawrence Berkeley National Laboratory. His research focuses on electrochemical technologies, including flow batteries, fuel cells, and solar-fuel generators. He received a Presidential Early Career Award for Scientists and Engineers (PECASE) in 2012 and the Charles W. Tobias Young Investigator Award from the Electrochemical Society in 2014.

These are not the final page numbers!

Although individual processes, such as the absorption of light and transport of carriers in semiconductors or electrocatalysts for water-splitting reactions, have been extensively modeled and simulated, only a few studies have modeled the whole operation of the system, which couples more than two processes.[6a, 7a,b, 8b, 10a, 13] For example, the effects that transport of the reaction products have on the absorption of light and transport of ions are often overlooked and not treated quantitatively. In addition, the properties of the ion transport across the membrane will have a strong influence on the pH conditions under which an efficient, safe system can be constructed. This in turn affects the choice of materials for the electrocatalysts and light absorbers that are active, stable, and compatible with such electrolytes and operating conditions. Moreover, most studies have treated the PEC systems as zero-dimensional (analytical) or one-dimensional.[14] Although this provides important trends and guidelines for solar-fuels research, the two-dimensional or three-dimensional effects in a real system play a critical role for understanding the operation of an actual prototype. For example, the the variation of current density with position along the photo-electrodes has a strong dependence on the cell dimensions and directly affects the overall STH conversion efficiency of the cell.[6a, 10, 13]

Advanced multiphysics, multidimensional modeling efforts, therefore, are based on detailed component models but require an important additional focus on the accurate definition of the boundary conditions and exchange of information between the device components. Conservation equations (e.g. for energy, charge, momentum, and mass) and transport equations (e.g. for electromagnetic waves and species) are solved with the accurate interface conditions for the component coupling.[15] A description of an interface can simply require continuity in fluxes or can also account for complex physical phenomena (e.g. electrochemical reactions or charge transport at the semiconductor–liquid interface). This coupling introduces an additional layer of complexity, because detailed component models accounting for a subset of physical phenomena might rely on the solution of another subset of equations (e.g. information about temperature distribution to provide detailed temperature-dependent material properties).[16] Consequently, coupled modeling efforts require additional external iterative solution steps, which generally increase the computational efforts and require special attention to ensure model robustness and convergence.

In this section, we examine the various underlying phenomena through the lens of a coupled system model. Such analysis includes not only a discussion about how to model, including relevant physics, but also key findings in the literature. Below, we examine each component and phenomenon in turn, and comment on the dominant interactions.

2.1. Semiconductors and the Transport of Light

The selection and optoelectronic design of the semi-conductor component of a PEC water-splitting device are critical to the overall performance of the device. The semi-conducting component generates the photovoltage and photocurrent required to drive the photoelectrochemical reactions through the generation of energized electrons by absorbing photons with energy greater than its band gap. In contrast to the design consideration of semiconductors in a photovoltaic device, the optical and electronic interactions between the semiconductors, protective layers, electrocatalysts layers, solution electrolytes, and product bubbles also play a vital role in optimizing the overall PEC performance. Although a comprehensive modeling and optimization tool that integrates all of the relevant optical and electronic effects has yet to be developed, significant advances have been made in determining the optimal band-gap combinations and the optimal band energetics for semiconductor materials using non-iterative models.[7b–d]
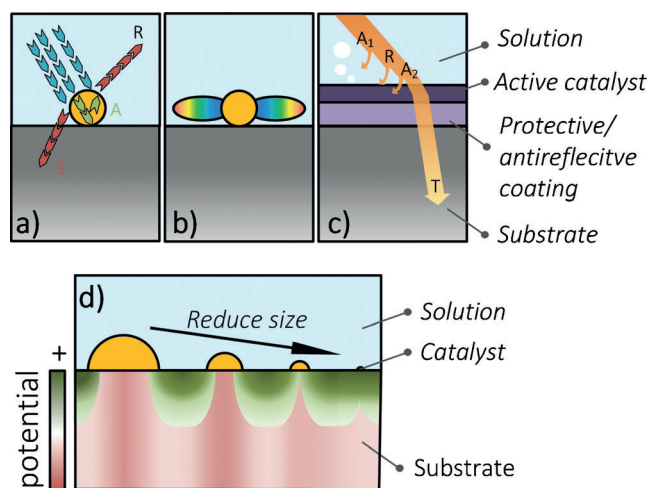
The selection of the optimal band-gap combinations of semiconductor materials in a solar-hydrogen device has different guiding principles than for a solid-state photovoltaic device. According to the Shockley–Queisser detailed-balance limit for photovoltaic efficiency, the photovoltage and photocurrent vary in opposing trends with the varying band-gap combinations, which results in an optimal semiconductor band-gap combination that maximizes the efficiency of the conversion of solar energy into electricity. However, in a solar-hydrogen device, the electrochemical potential difference between the HER and OER (i.e. 1.23 V under standard conditions) sets the lower boundary for the required photovoltage. A photovoltage greater than 1.23 V is required to overcome the various losses in the cell, including kinetics and transport, as the STH conversion efficiency only depends on the product of the photocurrent and the electrochemical potential of the reaction rather than that of the photocurrent and the photovoltage, as in photovoltaics. Maximum efficiencies for water splitting are achieved with dual-junction devices that combine photovoltages from two semiconductors in series to generate the photovoltage required for water splitting. The optimal band-gap combinations for a tandem cell structure in a solar-driven water-splitting cell have been evaluated.[7b–d, 14] For example, as shown in Figure 2, under simulated solar illumination with an air mass (AM) 1.5 solar spectrum, the optimal top/bottom semiconductor band-gap combination is 1.60/0.95 eV, which could yield, at the detailed-balance limit, a STH conversion efficiency of 29.7% in a system using planar Pt and RuO_x electrocatalysts and an optimized system design that minimizes the solution resistance (5 $Ohm\,cm^{-2}$).[7b] The optimal band-gap combination for the tandem photoabsorber is dependent on the performance of the electrocatalysts, the transport properties of the membrane separators and electrolyte, as well as the integrated device architecture.[7b,d, 17] The flexibility of the band-gap tuning in a tandem cell that could trade short-circuit photocurrent for open-circuit voltage can be utilized advantageously to compensate for the increase in the necessary voltage drops from various components in the system to achieve an optimized device efficiency.[7a,b]

The optical, electrical, and electrochemical interactions between the semiconductors, protective coatings, and electrocatalysts in an integrated PEC system present an additional dimension to optimization of light management and device
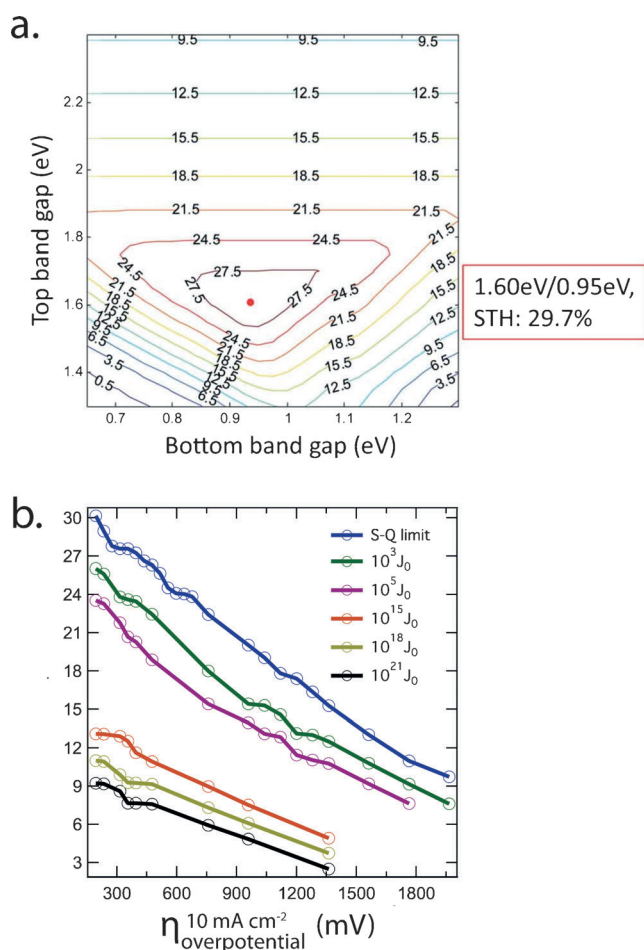
Figure 2. a). Contour plot of water-splitting efficiency for a dual-junction photoelectrochemical device as a function of the bottom and top semiconductor band gap; reproduced from Ref. [7b] with permission. b). Optimal STH conversion efficiency at all band-gap combinations as a function of the total overpotential for water splitting at 10 mA cm^{-2}. The reverse-saturation current densities for the photoabsorbers were swept from the Shockley–Queisser (S-Q) limit, J_0, to $10^{21}J_0$.[7a]

Figure 3. Schematic illustrations of optical couplings between catalysts and the light absorber. a) Far-field scattering for enhanced light absorption (blue arrow: incident light, red arrows: scattered and reflected light, green arrows: absorbed light, orange circle: metallic or dielectric nanoparticles). b) Near-field plasmon resonance for enhanced local energy absorption. c) Optical losses in a protected photoelectrode with uniform catalyst loading (A1: absorption loss by water layer, R: reflection loss at the substrate/solution interface and scattering loss by gas bubbles, A2: absorption loss by active catalysts, and T: total optical absorption by light absorber). d) Size-dependent inhomogeneous Schottky junction with a solution-induced inversion layer (IL); the green area shows the high potential barrier at the solution semiconductor interface, the red area shows the low potential barrier at the catalyst semiconductor interface.

performance that is non-existent in a PV-E system. In a discrete PV-E system, light management and the built-in potential in the PV component are independent of the electrolysis components. When an incident photon impinges on the surface of the PEC system, instead of being absorbed by the underlying semiconductor materials, the incident light could be modulated by the components in the optical pathway between the light source and the light absorber, including the electrolyte, bubbles, catalysts, protective coatings, and surface structures. This modulation could attenuate the light intensity and reduce the efficiency of light absorption by the light absorber through the redirection of light back to the light source in the form of reflection, including diffuse/back scattering and specular reflection (R in Figure 3a), as well as through the parasitic absorption by the various components (A in Figure 3a). In fact, such absorption of sunlight by water has been found to adversely affect the performance of solar-hydrogen cells, especially those that incorporate high-efficiency multijunction photoabsorbers.[7c]

Although the various components scatter or absorb light, this can possibly be used advantageously. When light is redirected forward by various components, this portion of light, known as deflected or forward-scattered light (S in Figure 3a), can be further absorbed by semiconductors through proper scattering. There are two types of scattering: elastic far-field scattering (Figure 3a) and near-field localized surface plasmon resonance (LSPR, Figure 3b).[18] Both scattering behaviors are strongly governed by the wavelength of the light, particle size/shape/morphology/density, polarization of the light, refractive index relative to surrounding media, and surface structures.[19] For example, nanoparticles at the front surface have been shown to enhance the absorption of light either from far-field scattering or near-field plasmonic resonance mainly on large-band-gap semiconductors ($E_g >$ 2 eV);[19b, 20] this strategy is less effective on small-band-gap semiconductors ($E_g < 2$ eV) due to their broader utilization of the spectrum. More importantly, the intimate contact between the semiconductors and the aqueous solution caused by the sparse loading of nanoparticles often causes stability issues. Therefore, various conformal protective coatings have been developed (Figure 3c).[21] In this design, properties such as the thickness of the solution layer,[7c] electrochromism in water-oxidation catalysts, catalyst loading, refractive index/thickness of protective coatings,[21c] and surface affinity to water all strongly affect the optical absorption of semiconductors. Thus, depending on the configurations of the scattering centers relative to the semi-

conductors, both forward and backward scattering can be utilized to enhance the absorption of light by the semiconductors, either at the front surface or at the back contact. Trade-offs between catalytic activity and parasitic absorption are discussed in the next section. Moreover, the evolution of gas bubbles at the catalyst surface during operation could also influence the spatial and temporal absorption properties of the semiconductors located underneath. Models that account for the above-mentioned optical losses and the consequent re-optimization of the band-gap combinations have yet to be developed. To date, only static models have been reported.

The loading of electrocatalysts and/or the incorporation of protective coatings not only affect the optical absorption of the semiconductors, but also the energetics in the semiconductors. Beyond the absorption and scattering effects of the electrocatalysts, as discussed, they also often reduce the attainable photovoltage of the system because of increased surface recombination sites and the low barrier heights at the semiconductor/catalyst junction as a result of the large thermionic emission-type majority-carrier recombination. The non-uniform barrier heights from a mixture of nanoscale catalyst/semiconductor and solution/semiconductor junctions over the photoelectrode surface result in the "pinch-off" effect (Figure 3d). This has been calculated theoretically and demonstrated experimentally for Ni nanoparticles coated on an n-type Si surface in a solution with a reversible redox couple.[22] However, the ability to exploit the "pinch-off" effect for water-splitting systems has yet to be investigated, as an advanced model that accounts for the variation in the height of the nanoscale barrier and optical absorption properties of the mixed semiconductor/catalyst and semiconductor/electrolyte system has yet to be developed.

2.2. Electrocatalysts

The electrochemical interfacial charge transfer between the semiconductor and the electrolyte solution (i.e. HER and OER) occurs at the electrocatalysts, which are traditionally supported on the semiconductor. Two junction types, the semiconductor/electrolyte junction and the "buried" solid-state junction, are typically modeled or are extensively employed experimentally.[23] The theoretical framework linking the semiconductor–liquid junctions, molecular donor–acceptor systems, and heterogeneous semiconductor–metal systems has long been established.[23c,d] The band energetics, available states in the solution, and the semiconductor and surface states can each influence the kinetic properties at the semiconductor electrodes for the HER and OER. The rate of charge transfer at the surface is coupled to the rate of carrier generation and separation in the semiconductor. Surface charges are critical in a liquid-junction cell to form the depletion region that affects charge transport. This characteristic comprises an important distinction from a buried-junction cell with an electrocatalyst on the surface, in which high rates of charge transfer between the absorber–catalyst and catalyst–electrolyte interfaces have the potential to decouple the rate of charge transfer from the properties of the semiconductor–electrolyte junction.

The charge-transfer reactions provide the boundary conditions necessary to couple the semiconductor and electrolyte domains. Both the desired electrochemical reaction (e.g. oxidation of H_2O to O_2 and H^+) and many undesired side reactions (e.g. surface recombination, crossover currents, corrosion of materials, etc.) should be considered when determining the device performance. Typically, such reactions are modeled using Butler–Volmer-type kinetic expressions,[15a] although microkinetic or reaction-mechanism models can be used, assuming one knows the various reaction steps and intermediates. Surface roughness and changes in cross-sectional area should also be considered, as they alter the geometric distribution of the current density along the surface of the electrode. Moreover, in an integrated PEC system, the catalyst performance is tied to the performance of the rest of the system (i.e. photoabsorbers, electrolytes, and membrane) due to the fact that the current is in series through them. In addition, additional layers may be included between the semiconductor and the electrocatalyst to stabilize and manage current distributions along the electrodes; these layers are typically modeled as conductive media using Ohm's law.

The impact of electrocatalytic properties on the STH conversion efficiency in an integrated cell has been investigated in several models.[7a,d,24] For a given photoabsorber system with a certain photodiode characteristic, depending on the position of the crossing point between the photodiode curve and the water-splitting load curve, the overall STH conversion efficiency could be extremely sensitive to the catalyst performance.[24] However, when the band-gap combination of the photoabsorbers can be optimized to provide the optimal photodiode characteristic for a series of electrocatalysts with different performances, only a relatively small decrease in the optimal STH conversion efficiency is calculated (ca. 1 % improvement of the optimally attainable STH conversion efficiency for a reduction of the overpotential at $10~mA\,cm^{-2}$ by 100 mV).[7a] Thus, the design and determination of ideal electrocatalysts cannot be uncoupled from that of photoabsorbers.

In terms of electrocatalyst placement, when electrocatalyst films are uniformly coated on the photoabsorber materials, the STH conversion efficiency of the device can be strongly affected by the parasitic absorption of the catalysts, which are either intrinsically optically opaque or electrochromic under electrolysis.[25] As a result, the optimal loading of catalysts in terms of thickness in these systems is as ultrathin (< 1 nm) films.[25a,26] Developing transparent and active catalyst films, such as microstructuring porous Pt films[27] or transparent NiO_x with suppressed electrochromism under electrolysis,[21a] is required to improve cell efficiency. Alternatively, catalyst loading in a form of random or regular arrays with very low geometric filling fractions (1–10 %) can minimize the sensitivity of the optimal STH conversion efficiency of cells to the detailed optical properties of the catalyst material.[28] However, the reduced catalytic area in the patterned catalyst design requires additional catalytic overpotential and/or additional transparent conductive layers, all of which may result in increased losses as a result of increased current flow through the electrocatalysts (i.e. higher

turnover frequency). Recent studies have shown that the use of low filling fractions and low catalyst loadings provide a viable method to lower the utilization of noble metals, such as Pt, when deployed at the terawatt scale.[28a]

2.3. Electrolytes

The electrolyte is critical component of a PEC device. It completes the electrochemical circuit and thus allows the device to operate and reactions to proceed. Mathematical modeling of the transport of species in electrolytes has different governing equations in infinitely dilute (< 0.1M), moderately dilute (0.1 to 1M), and concentrated electrolytes (> 1M).[15a,29] In an infinitely dilute electrolyte, every species moves independently and species interact only with the solvent (water). Here, the activity of each species can be approximated by its concentration. It should be noted that the vast majority of aqueous electrolytes of interest for solar-driven water-splitting cells can be treated by either dilute or moderately dilute models. There are three primary mechanisms by which species are transported: diffusion, migration, and convection, where the driving forces are the concentration gradient, electric field, and velocity field, respectively. In addition to the flux equations, equations that conserve mass, charge, momentum, and energy are also needed to model the system. For moderately dilute electrolytes, one must include the respective activity coefficient. For concentrated electrolytes, such as some membranes, where interactions between different species become important, advanced flux expressions that include friction coefficients and binary diffusion coefficients for multicomponent electrolytes need to be employed.[15a] In addition, for a solar-hydrogen cell with spatial and temporal variations in temperature, temperature gradients can drive mass fluxes (i.e. Soret effect) and mixing in the electrolyte.

The key for modeling and choosing electrolytes is understanding the interactions and polarization losses that determine the various ion concentrations at the electrocatalysts and the subsequent device performance. These concentrations stem from the transport of species (by migration and diffusion) and the resultant concentration gradients, which can be represented as a sum of the ohmic and diffusion losses or the concentration polarization. The ohmic loss is due to the resistance of the electrolyte, and the diffusion loss originates from the species gradient in the boundary layer near each electrode as a result of the electrochemical reactions. Below, we discuss the issues related to losses and interactions for liquid and membrane electrolytes in turn.

2.3.1. Liquid Electrolytes

Liquid electrolytes are ubiquitous for solar-hydrogen PECs, and contain multiple ions. Although their main function is to move protons (or hydroxide ions) between the two photoelectrodes, they often contain other species that can have an impact on the local environment of the electrocatalysts and hence the efficiency. The water-dissociation/

formation reaction [Eq. (1)] needs to be considered to model these systems.

$$H_2O \rightleftharpoons H^+ + OH^- \tag{1}$$

In addition, various types of pH buffers, such as acetate, phosphate, borate, and carbonate, are used in solar-driven water-splitting systems for operation at neutral or near-neutral pH values. Buffers can readily ionize or bind protons to balance pH changes in the electrolyte as a result of consumption/production of protons at the electrodes. The dissociation/association reaction of the buffer is given as Equation (2).

$$HA^- \rightleftharpoons H^+ + A^{2-}$$
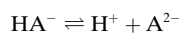
This buffer reaction is at thermal equilibrium if the rate of buffer dissociation is much faster than the rate of proton formation at the electrode. As the current density increases, the rate of proton formation can become comparable to or higher than the rate of buffer dissociation. In this case, a layer of electrolyte will form at each electrode, where the concentrations of buffer species are not in equilibrium with the bulk solution. The transport phenomena yield concentration gradients of the species that shift the concentrations of reacting species next to the electrode surfaces (e.g. protons, and hydroxide ions) away from those present in the bulk. These pH changes at the electrodes cause an increase in the equilibrium potential of the HER and OER, which has an impact on the electrocatalyst efficiency and associated kinetic overpotentials.

Three categories of aqueous electrolyte systems have been modeled and experimentally evaluated in recent reports on solar-driven water-splitting devices: 1) strongly acidic (i.e. 1M H_2SO_4) or strongly alkaline (i.e. 1M KOH) solutions, 2) near-pH-neutral electrolytes without membrane separators, 3) near-pH-neutral electrolytes with membrane separators. In strongly acidic or strongly alkaline solutions, the high conductivity, near unity transference numbers for protons or hydroxide ions, respectively, and small solar-photon-flux matched current densities result in minimal electrolyte losses during steady-state operation, even with membrane separators.

Modeling and simulation studies have shown that, with optimized system designs that include membranes to attenuate product gases crossover (see section 2.3.2), the total loss of polarization in the electrolyte and membrane can be < 100 mV at an operating current density > 20 mA cm^{-2}, that is, with STH conversion efficiencies in excess of 24%.[6a,13] However, strongly acidic or strongly basic electrolytes present significant stability challenges for the materials of the photoabsorbers and the electrocatalysts because most of the technologically relevant photoabsorber materials, including GaAs, InP, CdTe, and Si, are not stable, and there are few electrocatalyst materials that are stable, under such conditions.[30]

Alternatively, significant efforts have been devoted to systems that utilize electrolytes with neutral or near-neutral pH values.[3a,8a,31] For operation at near-neutral pH values

▌▌▌▌
↖↖ These are not the final page numbers!

www.angewandte.org

© 2016 Wiley-VCH Verlag GmbH & Co. KGaA, Weinheim

Angew. Chem. Int. Ed. **2016**, 55, 2 – 17

without membrane separators, STH conversion efficiency as high as 10% has been realized by using a set of discrete photovoltaic cells connected in series with an electrolysis cell.[3a] Simulation has also shown that the bubble-induced convective mixing in the cell enables the polarization losses associated with the pH gradients developed at the electrode surfaces to be reduced, and minimal transport loss in the electrolyte can be realized for efficient solar-driven water-splitting devices.[8b] However, the lack of a membrane separator presents significant challenges for robust gas separation and collection, especially for operation at elevated temperatures and pressures with spatial and temporal variations in the system. For example, a significant cross-over of products (up to 40% H_2 in the O_2 chamber) was observed experimentally in a monolithically integrated solar-driven water-splitting device without a membrane separator.[8a]

Operation at near-neutral pH values with a membrane separator has also been modeled and evaluated experimentally in a range of electrolytes and membrane combinations.[32] As discussed below, these membrane separators are most often ion-conduction polymers that nominally transport cations (i.e. protons) or anions (i.e. hydroxide ions) and, thus, are designed for use in strongly acidic or basic conditions.[8,32] However, recent modeling and simulation work has shown that under more neutral pH conditions, such systems result in significant concentration polarization because of electrodialysis effects resulting in large pH gradients (> 6 pH units) at the surface of the electrocatalysts, even at low operating current densities (ca. 1 mA cm^{-2}).[8b,32] Although sustainable photoelectrolysis has not been demonstrated at near-neutral pH operation with membrane separators, certain buffer-membrane systems, for example, imidazolium/imidazole[32] and bipolar membranes,[33] as well as recirculation architectures, have been explored.[31a]

2.3.2. Membrane Separator

Membrane electrolytes are key components of PEC devices, as they allow for ionic transport but block cross-over of the gas product. Although they are typically used alongside liquid electrolytes, vapor-feed devices utilize ion-conducting membranes as the sole electrolyte[10a,34] (see Section 3.4). Comprehensive reviews and textbooks have discussed specific material systems used as separators for water electrolysis, including proton- and anion-exchange membranes.[35] Regardless of the pH value of the electrolyte, the material systems can be broadly categorized as microporous or ionic. Porous separators are a more mature technology, with glass and fiber-based diaphragms being used in fields such as the chlor-alkali industry. The ionic separators of interest to solar fuels are typically polymeric membranes because of the need to have high ionic conductivity near ambient temperature and to limit cross-over arising from pressure gradients. Various approaches to separate products without the use of a separator have been explored,[31b,36] although these typically result in large voltage drops because of ohmic losses.[8a]

Ion transport in the separator follows the same multicomponent diffusion equations that are used to model bulk electrolyte transport, except separators may require the use of equations for a concentrated solution.[15a] Inside the separator, the diffusion coefficients are likely to differ from their bulk values. In the case of a porous separator, corrections arising from porosity and tortuosity should be considered. Although porosity is a tunable parameter to some extent, both ions and gases are affected in the same way. This presents a fundamental limitation for porous separators: a decrease in gas permeability will have a corresponding decrease in ionic conductivity. Since gas transport across the separator is undesirable, as it results typically in a parasitic loss of product and a drop in current efficiency,[37] and since small pressure gradients can cause significant cross-over, this requires one to utilize polymer membranes instead of microporous ones.[13,38]

In the case of a membrane separator, interactions between the polymer and the species in solution may also have an effect, yielding different solubilities and diffusivities for ions and gases. Various transport mechanisms can occur (e.g. vehicular and hopping-like mechanisms, such as the Grotthuß mechanism); therefore, the density and chemical nature of the functional groups along the polymer backbone can affect ion transport,[39] and care should be taken to measure or estimate the needed transport properties accurately.[40] These transport properties may also be affected by non-ideal behavior arising from morphological changes when switching liquid electrolytes or varying the hydration.

Another important consideration is how to handle the interface between the separator and the bulk solution. The material balance typically ignores any interfacial mass-transfer resistance, which means one can equate the electrochemical potential for each species across the interface as a boundary condition. For polymer membranes, this leads to a discontinuity in the potential (called the Donnan potential) as a result of the charged groups on the polymer, which should be accounted for.[37] Care should be taken when defining the potential to be used along with the reference states for electrochemical potentials. In most cases, the Debye length is short enough that membranes can be modeled using the assumption of electroneutrality, but the Poisson and Nernst–Planck equations can be used if necessary.

Creative strategies are needed to design membranes with ideal transport properties for solar-fuel applications. Some strategies have involved modifying the annealing treatment of Nafion[41] or designing block copolymers with tethered ionic-liquid functional groups.[42] It may also be possible to borrow concepts from related fields including from fuel-cell research, where past efforts have looked at polymer–composite blends[43] and manipulation of the chemical composition and chain length.[44] As mentioned above, electrodialysis effects can have a great impact on device performance at near-neutral pH values and/or with buffers. Near-neutral membranes (e.g. imidazolium/imidazole) or the use of bipolar membranes have shown some promise in reducing the electrodialysis effect by back diffusion of the neutral buffer species in the membrane. Bipolar membranes are interesting in that they allow for sustainable cell reactions at two electrolytes with different pH values.[33] Bipolar membranes have been widely used in the electrodialysis industry for

producing concentrated acid and base solutions and desalinating salt water, but solar-hydrogen devices that incorporate bipolar membranes were not modeled and evaluated experimentally until very recently.[33,45] A range of electrolyte combinations with different pH gradients exhibited sustainable solar-driven water-splitting reactions under steady-state conditions. A recent study with bipolar membranes has also shown that large-area ($> 1 \, cm^2$) III-V tandem photoabsorbers incorporating only earth-abundant electrocatalysts exhibited > 100 h of device stability at 10 % STH conversion efficiency, with a steady-state pH gradient of pH 9.3/pH 0.[46] However, the resistive loss, as well as the additional kinetic overpotential associated with water dissociation at the cation/anion internal membrane interface in the bipolar membrane constituted a voltage loss of more than 400 mV in the system.[46] Future studies that involve improving the ohmic resistive loss in the bipolar membrane system as well as investigations of weak-acid membrane systems and novel membrane structures and chemical properties could potentially offer a more efficient and stable operation of solar-hydrogen cells.

3. Cell Design and Implementation

The performance of integrated solar-driven water-splitting devices is not only dependent on the properties and performances of the individual components, as discussed in the previous sections, but also on component integration, overall device architecture, and the operating conditions of the system. Regardless of the various device configurations and operational conditions, the performance metrics of integrated solar-hydrogen devices can be summarized using the STH conversion efficiency and device stability, scalability, and safety. The true STH conversion efficiency of a full device should be based on the total amount of H_2 and O_2 produced and collected as a function of the incoming irradiance. In practice, however, this is typically calculated from the photocurrent density that is attained under illumination when the anode and cathode are shorted together, assuming a 100 % faradaic yield for the generation and collection of H_2 and O_2. The former method is more rigorous and accurate, especially for fully integrated, wireless devices, and is recommended. The stability of a practical solar-hydrogen cell should be evaluated by measuring the rate of hydrogen production under realistic conditions that include a diurnal cycle of solar illumination and varying temperature conditions. As a consequence of the small size of typical laboratory-scale photoactive substrates and the lack of long-term stability in fully integrated devices, the stability is often characterized by monitoring the photocurrent density as a function of time without any external bias for continuous operation under simulated solar illumination. The scalability of the device is often evaluated by the abundance and perceived cost of the chemical elements that are required to construct the cell, while the safety of the device is often evaluated by whether the device has a robust mechanism for the separation and collection of product gas. In this section, a range of device architectures (Figure 4) that could potentially meet all four
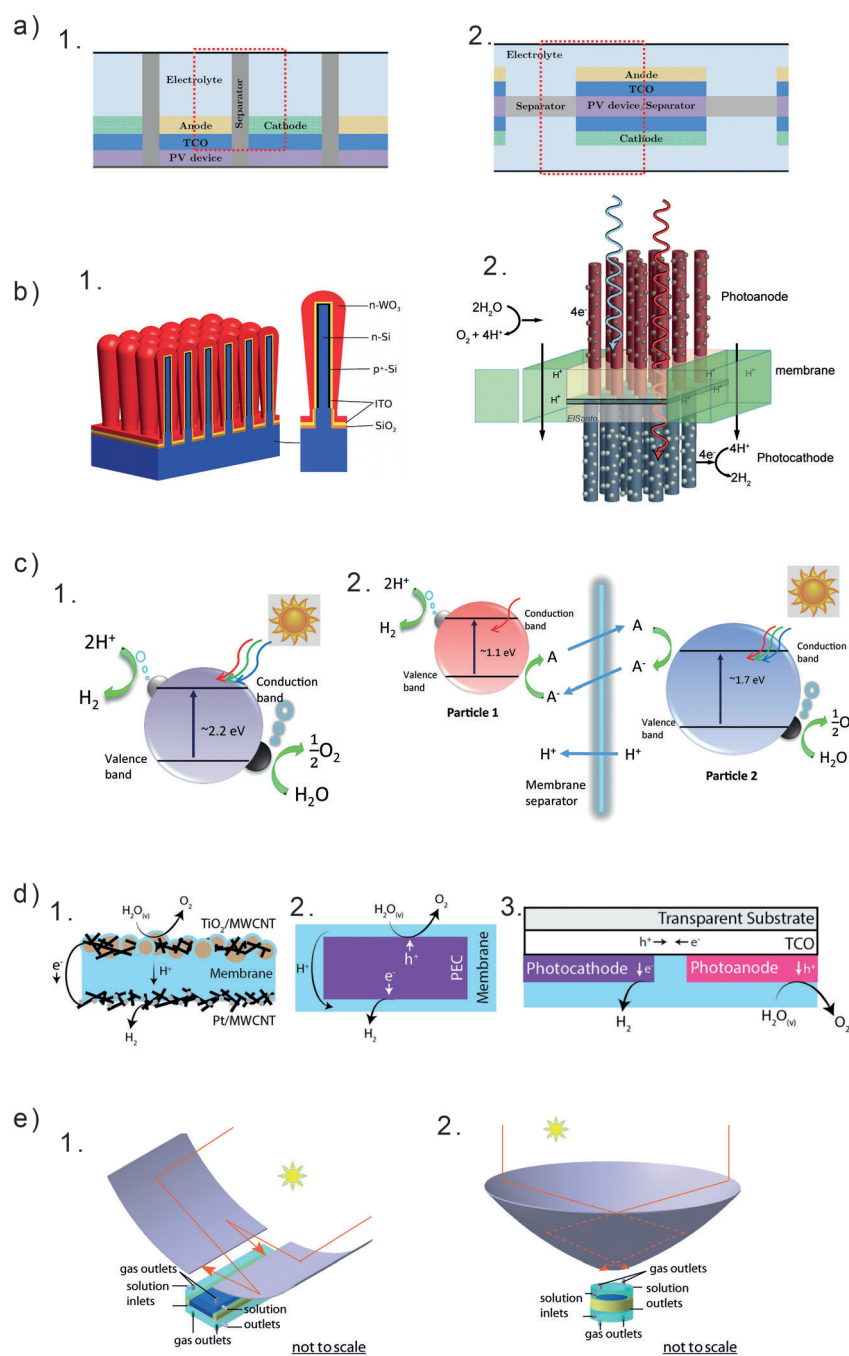
performance metrics: efficiency, stability, scalability, and safety will be reviewed, including nontraditional designs, with a focus on interactions at the cell level and subsequent modeling and simulation descriptions.

3.1. Planar Design

One class of PEC reactor architectures utilizes macroscopic planar arrays of photoelectrodes (Figure 4a). These photoelectrodes simultaneously provide functionality for the absorption of solar irradiation, electron and hole transport, as well as electrochemical reactions, and are often multicomponent arrangements of nano-/microstructured (ultra)thin layers[11d,21f,47] composed of the active photoelectrode, buried photovoltaic cells (traditional heterojunction cells or dye-sensitized solar cells),[48] protection and passivation layers, electrocatalytic layers, and ohmic or tunnel-junction layers. The planar electrodes have to be in contact with electrolyte to provide the functionality needed for a working PEC cell. Additionally, a practical design requires a semipermeable membrane to ensure product separation, maximum production collection efficiency, and device safety, all while enabling rapid ionic conduction.[8a,21f] Modeling has been key in establishing the design requirements of the planar electrodes, electrolyte, and separator. For an optimized multicomponent photoelectrode, the design guidelines need to ensure optimized absorption of radiation by the photoelectrode(s) and efficient transport of ionic charge in the electrolytes and the membrane separators.

The majority of the designs based on planar photoelectrodes can be categorized as back-to-back (Figure 4a1) and side-by-side (Figure 4a2) designs. The back-to-back PEC design often contains photoabsorbers with dual-junction or triple-junction semiconductor materials to provide enough voltage to drive net water splitting. Although the back-to-back design could in principle achieve the Shockley–Queisser efficiency limit for a tandem-junction or triple-junction cell, this design has very stringent requirements in terms of materials. The multijunction photoabsorber materials need to have complementary band gaps and similar lattice constants for epitaxial cell growth. As a result, the multijunction photoabsorber component incorporated in the back-to-back design often contains conventional photovoltaic semiconductors (e.g. Si, GaAs, InP, CdTe, CIGS (copper indium gallium selenide)). Metal oxides and other nonconventional photoabsorbers typically present difficulties in multijunction cell architectures because of a lack of a lattice-matched semiconducting partner with a complementary band gap, or the inability to accommodate a transparent tunnel junction, or both. Alternatively, the side-by-side design significantly relaxes the material constraints by the use of two photoactive electrodes electrically connected in series, but arranged in parallel with respect to the direction of the incident light. The lattice-matching constraints and the need for optically transparent electrical contacts between the photocathode and photoanode are not applicable to the side-by-side design. Moreover, the difference in the catalytic overpotential for the HER and OER and the current-matching constraints

▮▮▮▮ www.angewandte.org

◂◂ These are not the final page numbers!

© 2016 Wiley-VCH Verlag GmbH & Co. KGaA, Weinheim

Angew. Chem. Int. Ed. **2016**, 55, 2 – 17

Figure 4. Schematic illustrations of various prototype architectures. a) Macroscopic planar design. 1. Side-by-side PEC design; reproduced from Ref. [13] with permission. 2. Back-to-back PEC design; reproduced from Ref. [13] with permission. b) Microwire and microstructured designs. 1. Core–shell tandem junction microwire design; reproduced from Ref. [55] with permission. 2. Tandem junction microwire design; reproduced from Ref. [79] with permission. c) Particle-suspension reactors. 1. Type 1 single-vessel reactor, 2. Type 2 dual-vessel reactor. d) Vapor-feed designs. 1. A photoactive MEA design. 2. A membrane-encapsulated PEC design. 3. A side-by-side microfluidic PEC design. e) Solar-concentrator-coupled PEC design. 1. A two-dimensional "trough" design; reproduced from Ref. [10b] with permission. 2. Three-dimensional "bubble wrap" design; reproduced from Ref. [10b] with permission.

a single-junction absorber unless an efficient spectral-splitting method can be implemented in the cell architecture. In addition to the monolithic wireless device design, a variety of laboratory-scale demonstrations contained only a photoanode[11d, 47a, 49] or a photoanode,[50] wired to a dark counter electrode. Simulations of the differences between the wired and wireless back-to-back designs showed that the design of the wired device ensured shorter paths for ionic conduction compared to the wireless design.[51] When the dimensions of the electrodes are not well designed, the wireless design can exhibit higher resistive losses than the wired design owing to the order-of-magnitude larger electronic conductivity of wires compared to the ionic conductivity in electrolytes.

Multiphysics modeling has enabled computed efficiency evaluations of the two planar cell architectures. The size of the electrodes, the distance between the OER and the HER catalysts, and the detailed geometry for the membrane separator and solution channels play significant roles in minimizing the transport loss in the electrolyte and membrane for efficient solar water splitting. Since both the path length for ion transport and the conductivity of the electrolyte can limit the efficiency of a PEC device, a practical (large-scale) plant cannot be based on large planar monolithic photoabsorbers, as often proposed,[5b, 52] or as suggested by the experience of scaling photovoltaic devices. Spatially resolved computational models[6a, 13] have suggested that typical electrode dimensions should lie in the range of millimeters to centimeters for efficient operation of a PEC device.

3.2. Microwire and Microstructured Designs

The design criteria for microwire and microstructured solar-driven water-splitting devices (Figure 4b) are identical to those for planar architectures, with the difference being that the active device unit cells are now on the size of micrometers rather than centimeters. Hence, the modeling analysis and approaches remain the same. Additionally, the ultimate metric for success—a stable STH conversion efficiency at low cost and safe operation—remains the same, irrespective of the architecture of the active

between the photocathode and the photoanode can also be accommodated by tuning the ratio of the surface areas of the photoelectrodes. However, the attainable efficiency of the side-by-side design is limited to the theoretical efficiency of

These are not the final page numbers!

component. Thus, two critical questions are: what is the risk profile associated with the potential advantages of micro-structured solar-driven water-splitting devices over planar equivalents if everything goes perfectly, and what are the potential disadvantages given the thermodynamic and engineering constraints?

Many potential benefits of microstructured architectures compared to planar architectures for the production of fuels from solar energy have been enumerated, but no quantitative advantage, in terms of economics and/or performance, has been shown in any real system. To date, all microwire and microstructured devices that perform unassisted solar-driven water splitting have significantly lower STH conversion efficiencies than their planar equivalents. This performance deficit is not unique to unassisted solar-driven water-splitting devices; it is also the case for single-junction photovoltaic and PEC devices.

The potential benefits of microstructured designs compared to planar ones include lower material usage,[53] lower requirements for material purity,[47c] minimized ionic-transport distance,[13,54] robustness against catastrophic device failure, and fundamentally different module designs that affect the balance-of-systems requirements.[55] However, challenges include the increased complexity of epitaxial growth on the nontraditional crystallographic surface terminations present, as has been used for state-of-the-art planar designs, and the increased fabrication complexity, in general.

Single-junction photovoltaic demonstrations using Si, InP, GaAs, and CdS microwire arrays have champion array efficiencies of 7.9, 13.8, 7.6, and 6%, respectively.[56] Near-complete light absorption above the band gap has been achieved in Si microwire arrays by introducing scattering elements into the unoccupied space within the microwire array.[53] Many, if not all, of these photovoltaic demonstrations are directly applicable to solar-driven water-splitting devices, as they could constitute one of the two or three junctions required for efficient operation, although a protective coating is necessary in most cases because of the instability of the semiconductors under PEC operating conditions, as noted above. Single-junction PEC applications using microstructured arrays have focused primarily on the HER. For example, single-junction pn^+-Si devices coated with an electrocatalyst such as Pt have shown 5.8% efficiency for hydrogen evolution.[11g,i]

Attempts to design and fabricate tandem-junction microstructured devices have been challenging because of the complex nature of the exposed crystal facets on which a material must be grown. Two routes have been investigated: epitaxial growth of high-performance compound semiconductors (GaP, GaInP),[57] and growth of defective, nano-/microcrystalline materials that may provide intrinsic advantages in terms of stability over the known higher performance materials,[11j,55,58] where a maximum STH conversion efficiency of 0.12% has been reported.[11j] For microstructured devices to achieve more than just scientific interest, clear, quantitative performance and/or economic advantages over planar equivalents must be demonstrated including perhaps impacts on balance-of-systems requirements and costs.

3.3. Particulate Designs

A possible subset of microstructured designs are particulate-suspension designs, which remove the panel motif adopted from photovoltaics and have the potential to decrease balance-of-systems costs significantly.[5c,59] Two types of particle-based PEC systems, termed a Type 1 reactor for a single-vessel reactor (Figure 4c1) and a Type 2 reactor for a dual-vessel reactor (Figure 4c2), have been proposed conceptually and demonstrated experimentally at different levels of device integration. For the Type 1 reactor, single particle systems, including $In_{1-x}Ni_xTaO_4$,[60] $(Zn_{1+x}Ge)(N_2O_x)$ solid solution,[61] $(Ga_{1-x}Zn_x)(N_{1-x}O_x)$ solid solution,[62] CoO[63] and C_3N_4/C-dots,[64] as well as tandem-particle systems, including $SrTiO_3$:Rh//$BiVO_4$[65] and nitrogen-doped graphene oxide (NGO)[66] that are electrically connected with a solid-state electron mediator have been investigated. The STH conversion efficiency in the demonstrated and stable Type 1 reactor systems is often low ($<2\%$). This low efficiency, coupled with a lack of a robust product-separation mechanism, presents a significant challenge for large-scale implementation of such a device design.

In the Type 2 reactor, two noncontacting particles for a tandem cell are employed with a separator for separation of the product gas and redox-mediator transport. The Type 2 reactor leverages the tandem design and could achieve a theoretical STH conversion efficiency of about 25% with band-gap combinations of approximately 1.7 eV/1.1 eV as determined through modeling.[7b] The redox mediator, such as those based on iodine,[67] iron,[68] or cobalt,[69] could provide the necessary ionic transport between the two electrochemical compartments (i.e. it acts as a molecular or ionic wire). One of the major challenges for the Type 2 reactor design is the redox selectivity at the respective catalyst sites for the HER and OER. For example, photodriven proton reduction on the HER particle has to be much more selective than reduction of the redox mediator, despite the fact that reduction of the redox mediator is often much more thermodynamically favorable. Therefore, strategies that involve the selective transport of protons and H_2 through porous oxides[70] or composite shells[71] have been employed to minimize the reduction of O_2 at the catalyst surface. Other challenges include large distances for transport of the redox mediator in the solution and the membrane electrolyte, pH gradients between the two reactor vessels, and uncertain dimensions for the reactor construct; there is still a need for significant modeling and simulation studies as well as experimental validation to optimize these device designs.

3.4. Vapor-Feed Design

As discussed in Section 2.3, ion-conducting polymers can function as solid electrolytes in a solar fuel device, thereby bypassing the need for liquid electrolyte and resulting in a solid-state hydrogen generator that operates with a water-vapor feed. Operation with vapor has several advantages: the elimination of light management and catalysis limitations from the formation of bubbles at the reaction sites, elimi-

www.angewandte.org

These are not the final page numbers!

© 2016 Wiley-VCH Verlag GmbH & Co. KGaA, Weinheim

Angew. Chem. Int. Ed. **2016**, *55*, 2–17

nation of the use of corrosive liquid electrolytes on a large scale, and an overall simplification of the device design and operation.[72] These advantages come at the expense of operation under dilute water feeds, which reduce the flux of water molecules to the (photo)catalytic centers and ultimately can limit the device performance. In addition, in the absence of a liquid electrolyte, ionic transport between the cathode and anode compartment is more challenging. These requirements are similar to those encountered in catalyst layers of membrane-electrode assemblies for the electrolysis of water.[35b]

The electrolysis of water using commercially available membrane-electrode assemblies with a water-vapor feed has demonstrated operating current densities on the order of tens of mA cm^{-2}, which is sufficient for the operation of a broad range of solar-driven water-splitting devices.[73] Reduced current density and cell failure using vapor feed are often caused by limitations in the mass transport of the reactant water and dehydration of the membrane electrolyte resulting in increased ohmic losses. A light-driven demonstration system was reported that used a membrane-electrode assembly with photoactive TiO$_2$ nanoparticles incorporated into the membrane layer (Figure 4d1). Although the achieved operational current density was low in the TiO$_2$-based water-vapor device, the integrated absorber-in-membrane type design could lead to low-cost, high-performing systems if the activity of the materials could be improved. Similar absorber-in-membrane architectures that incorporate semiconducting microwires have also been proposed, where the electrical connectivity of the device is achieved through the microwires that cross through the membrane.[55,74]

Recent modeling studies have also provided guidelines for the design of efficient vapor-fed solar-hydrogen devices, where the ionomer encapsulates the photoelectrochemical components (Figure 4d2). Critical device dimensions that lead to optimal water, hydrogen, and oxygen transport have been identified in various cell configurations. To achieve a current density of about 10 mA cm^{-2} in the membrane-encapsulated PEC device, the thickness of the ionomer film needs to remain below 5 μm to avoid the formation of hydrogen or oxygen bubbles at the catalyst/membrane interface and the subsequent delamination between the membrane and the electrode.[10a] As a consequence of the required small, thin membrane layer, a small electrode width (< 300 μm) is also necessary to maintain low ohmic resistive losses in the electrolyte. Alternatively, incorporation of a structured membrane that balances the gas and ionic transport allows the maximum electrode width to be increased to dimensions as large as a few millimeters. Furthermore, as water is consumed at the anode, anisotropies in the hydration level of the polymer electrolyte arise,[34c] which can further increase its resistance, especially as the ionomer is confined in a thin-film morphology that constrains its water uptake.[75] These dehydration effects have been recently demonstrated in a microfluidic water-vapor electrolyzer (Figure 4d3).[76] As the device operated, the ohmic resistance increased because of the loss of water from the ionomer, which led to lower current densities at the steady state. Overall, water-vapor feeds are promising for solar-fuel generators, assuming that cost metrics

and the correct current-density operating regime are amenable.

3.5. Solar-Concentrator-Coupled PEC Design

Cell designs that utilize a low-multiple concentrating solar collector (Figure 4e), such as a 10 × concentrator, have great promise for large-scale, distributed splitting of water by solar energy. A principal advantage of a sunlight-concentrating design is the potential reduction in the amount of materials, thereby resulting in a significant reduction in the system cost.[5b,c] Typically, these devices use a planar architecture, although any of the above designs could ideally be coupled with a concentrator. However, the increased insolation could have deleterious effects on the stability and efficiency, as a consequence of such issues as increased operating temperatures and current densities. The operational photocurrent density and the open-circuit voltage of the photoabsorber materials, the catalytic performance of the electrocatalysts, and ionic transport in the electrolyte all have convolved dependences on the operational temperature and illumination intensity. For example, although increases in the illumination intensity increase the photocurrent density and concomitantly improve the open-circuit voltage,[77] the resultant increased current density would also, however, result in an increase in the ohmic losses of the cell, as well as possibly in the reaction overpotentials.[29]

As a consequence of the complex interactions, there have been attempts to model and build wireless, optically concentrating solar-driven water-splitting devices.[10b,78] Multiphysics modeling of the steady-state operation of trough-like and axisymmetric 10x solar-driven water-splitting devices found that, for a design utilizing planar architecture, the absorber widths need to be reduced (to a few millimeters) to avoid unacceptable efficiency losses from the ohmic drop in the liquid electrolyte. Despite this, a theoretical STH conversion efficiency in excess of 29 % could be achieved using tandem-junction light absorbers and state-of-the-art electrocatalysts. Beyond just steady-state operation, the daily and location-dependent variation in illumination intensity (which is compounded with the finite acceptance angle of the concentrating lens) and subsequent thermal increases could result in safety or lifetime issues. For example, hot days with no wind could result in temperatures above the boiling point of the electrolyte, or, at night in cold weather, the electrolyte could freeze. To analyze such real-world concerns, not only for concentrating systems but also nonconcentrating ones, a robust modeling approach that considers the concentration, PEC behavior, local weather and insolation conditions, as well as heat balances must be implemented; something that would benefit the field.

4. Summary

Significant advances have been made in recent years in the modeling- and simulation-guided development of integrated solar-driven water-splitting devices. Multidimensional

These are not the final page numbers! ↗↗

multiphysics models that account for various photoelectrochemical processes have provided design guidelines for semiconductors, electrocatalysts, and both liquid and membrane electrolytes. This Review covered the guiding principles and key findings of these activities, with a focus on their interactions. In addition, modeling and simulation have also revealed a range of viable device architectures that can accommodate efficient, stable, scalable, and safe solar-driven water-splitting reactions. Although devices are being quantitatively designed and implemented, various needs still remain in terms of both capturing more complicated physics (e.g. thermal effects and bubble formation) as well as experimentally demonstrating the various trade-offs in operation.

[1] a) H. B. Gray, *Nat. Chem.* **2009**, *1*, 7; b) N. S. Lewis, D. G. Nocera, *Proc. Natl. Acad. Sci. USA* **2006**, *103*, 15729–15735; c) R. E. Blankenship, D. M. Tiede, J. Barber, G. W. Brudvig, G. Fleming, M. Ghirardi, M. R. Gunner, W. Junge, D. M. Kramer, A. Melis, T. A. Moore, C. C. Moser, D. G. Nocera, A. J. Nozik, D. R. Ort, W. W. Parson, R. C. Prince, R. T. Sayre, *Science* **2011**, *332*, 805–809.

[2] a) M. G. Walter, E. L. Warren, J. R. McKone, S. W. Boettcher, Q. X. Mi, E. A. Santori, N. S. Lewis, *Chem. Rev.* **2010**, *110*, 6446–6473; b) J. W. Ager, M. R. Shaner, K. A. Walczak, I. D. Sharp, S. Ardo, *Energy Environ. Sci.* **2015**, *8*, 2811–2824.

[3] a) C. R. Cox, J. Z. Lee, D. G. Nocera, T. Buonassisi, *Proc. Natl. Acad. Sci. USA* **2014**, *111*, 14057–14061; b) J. S. Luo, J. H. Im, M. T. Mayer, M. Schreier, M. K. Nazeeruddin, N. G. Park, S. D. Tilley, H. J. Fan, M. Gratzel, *Science* **2014**, *345*, 1593–1596.

[4] a) A. Dukic, M. Firak, *Int. J. Hydrogen Energy* **2011**, *36*, 7799–7806; b) R. E. Clarke, S. Giddey, F. T. Ciacchi, S. P. S. Badwal, B. Paul, J. Andrews, *Int. J. Hydrogen Energy* **2009**, *34*, 2531–2542.

[5] a) T. Lipman, DOE, **2011**; b) B. A. Pinaud, J. D. Benck, L. C. Seitz, A. J. Forman, Z. B. Chen, T. G. Deutsch, B. D. James, K. N. Baum, G. N. Baum, S. Ardo, H. L. Wang, E. Miller, T. F. Jaramillo, *Energy Environ. Sci.* **2013**, *6*, 1983–2002; c) B. D. James, G. N. Baum, J. Perez, K. N. Baum, "Technoeconomic Analysis of Photoelectrochemical. (PEC) Hydrogen Production", DOE Report, **2009**.

[6] a) S. Haussener, S. Hu, C. Xiang, A. Z. Weber, N. Lewis, *Energy Environ. Sci.* **2013**, *6*, 3605–3618; b) J. R. McKone, N. S. Lewis, H. B. Gray, *Chem. Mater.* **2014**, *26*, 407–414.

[7] a) Y. Chen, S. Hu, C. Xiang, N. S. Lewis, *Energy Environ. Sci.* **2015**, *8*, 876–886; b) S. Hu, C. X. Xiang, S. Haussener, A. D. Berger, N. S. Lewis, *Energy Environ. Sci.* **2013**, *6*, 2984–2993; c) H. Döscher, J. F. Geisz, T. G. Deutsch, J. A. Turner, *Energy Environ. Sci.* **2014**, *7*, 2951–2956; d) L. C. Seitz, Z. Chen, A. J.

Forman, B. A. Pinaud, J. D. Benck, T. F. Jaramillo, *ChemSusChem* **2014**, *7*, 1372–1385; e) A. Berger, R. A. Segalman, J. Newman, *Energy Environ. Sci.* **2014**, *7*, 1468–1476.

[8] a) J. Jin, K. Walczak, M. R. Singh, C. Karp, N. S. Lewis, C. Xiang, *Energy Environ. Sci.* **2014**, *7*, 3371–3380; b) M. R. Singh, K. Papadantonakis, C. X. Xiang, N. S. Lewis, *Energy Environ. Sci.* **2015**, *8*, 2760–2767.

[9] K. Walczak, Y. K. Chen, C. Karp, J. W. Beeman, M. Shaner, J. Spurgeon, I. D. Sharp, X. Amashukeli, W. West, J. Jin, N. S. Lewis, C. X. Xiang, *ChemSusChem* **2015**, *8*, 544–551.

[10] a) C. Xiang, Y. Chen, N. S. Lewis, *Energy Environ. Sci.* **2013**, *6*, 3713–3721; b) Y. K. Chen, C. X. Xiang, S. Hu, N. S. Lewis, *J. Electrochem. Soc.* **2014**, *10*, F1101–F1110.

[11] a) K. Fujii, S. Nakamura, M. Sugiyama, K. Watanabe, B. Bagheri, Y. Nakano, *Int. J. Hydrogen Energy* **2013**, *38*, 14424–14432; b) T. J. Jacobsson, V. Fjallstrom, M. Sahlberg, M. Edoff, T. Edvinsson, *Energy Environ. Sci.* **2013**, *6*, 3676–3683; c) O. Khaselev, A. Bansal, J. A. Turner, *Int. J. Hydrogen Energy* **2001**, *26*, 127–132; d) O. Khaselev, J. A. Turner, *Science* **1998**, *280*, 425–427; e) S. Licht, B. Wang, S. Mukerji, T. Soga, M. Umeno, H. Tributsch, *J. Phys. Chem. B* **2000**, *104*, 8920–8924; f) G. Peharz, F. Dimroth, U. Wittstadt, *Int. J. Hydrogen Energy* **2007**, *32*, 3248–3252; g) S. W. Boettcher, E. L. Warren, M. C. Putnam, E. A. Santori, D. Turner-Evans, M. D. Kelzenberg, M. G. Walter, J. R. McKone, B. S. Brunschwig, H. A. Atwater, N. S. Lewis, *J. Am. Chem. Soc.* **2011**, *133*, 1216–1219; h) M. R. Shaner, S. Hu, K. Sun, N. S. Lewis, *Energy Environ. Sci.* **2015**, *8*, 203–207; i) E. L. Warren, J. R. McKone, H. A. Atwater, H. B. Gray, N. S. Lewis, *Energy Environ. Sci.* **2012**, *5*, 9653–9661; j) C. Liu, J. Tang, H. M. Chen, B. Liu, P. Yang, *Nano Lett.* **2013**, *13*, 2989–2992; k) S. A. Bonke, M. Wiechen, D. R. MacFarlane, L. Spiccia, *Energy Environ. Sci.* **2015**, *8*, 2791–2796.

[12] a) H. Ahmad, S. K. Kamarudin, L. J. Minggu, M. Kassim, *Renewable Sustainable Energy Rev.* **2015**, *43*, 599–610; b) A. A. Ismail, D. W. Bahnemann, *Sol. Energy Mater. Sol. Cells* **2014**, *128*, 85–101; c) M. Ni, M. K. H. Leung, D. Y. C. Leung, K. Sumathy, *Renewable Sustainable Energy Rev.* **2007**, *11*, 401–425; d) S. J. A. Moniz, S. A. Shevlin, D. J. Martin, Z. X. Guo, J. W. Tang, *Energy Environ. Sci.* **2015**, *8*, 731–759; e) D. M. Fabian, S. Hu, N. Singh, F. A. Houle, T. Hisatomi, K. Domen, F. E. Osterlohf, S. Ardo, *Energy Environ. Sci.* **2015**, *8*, 2825–2850; f) Z. S. Li, W. J. Luo, M. L. Zhang, J. Y. Feng, Z. G. Zou, *Energy Environ. Sci.* **2013**, *6*, 347–370; g) J. T. Li, N. Q. Wu, *Catal. Sci. Technol.* **2015**, *5*, 1360–1384; h) X. B. Chen, S. H. Shen, L. J. Guo, S. S. Mao, *Chem. Rev.* **2010**, *110*, 6503–6570.

[13] S. Haussener, C. Xiang, J. M. Spurgeon, S. Ardo, N. S. Lewis, A. Z. Weber, *Energy Environ. Sci.* **2012**, *5*, 9922–9935.

[14] J. R. Bolton, S. J. Strickler, J. S. Connolly, *Nature* **1985**, *316*, 495–500.

[15] a) J. Newman, K. E. Thomas-Alyea, *Electrochemical Systems*, 3rd ed., Wiley, New York, **2004**; b) R. B. Bird, W. E. Stewart, E. N. Lightfoot, *Transport Phenomena*, 2nd ed., Wiley, New York, **2002**.

[16] S. Y. Tembhurne, M. Dumortier, S. Haussener in *15th International Heat Transfer Conference*, Kyoto, Japan, **2014**.

[17] H. Doscher, J. Geisz, T. Deutsch, J. A. Turner, *Energy Environ. Sci.* **2014**, *7*, 2951–295.

[18] H. A. Atwater, A. Polman, *Nat. Mater.* **2010**, *9*, 205–213.

[19] a) M. B. Cortie, A. M. McDonagh, *Chem. Rev.* **2011**, *111*, 3713–3735; b) C. Clavero, *Nat. Photonics* **2014**, *8*, 95–103.

[20] a) M. Murdoch, G. I. N. Waterhouse, M. A. Nadeem, J. B. Metson, M. A. Keane, R. F. Howe, J. Llorca, H. Idriss, *Nat. Chem.* **2011**, *3*, 489–492; b) S. Mubeen, J. Lee, N. Singh, S. Kramer, G. D. Stucky, M. Moskovits, *Nat. Nanotechnol.* **2013**, *8*, 247–251.

[21] a) K. Sun, Y. Kuang, E. Verlage, B. S. Brunschwig, C. W. Tu, N. S. Lewis, *Adv. Energy Mater.* **2015**, 1402276; b) K. Sun, M. T.

■■■■ www.angewandte.org **⤢⤢** These are not the final page numbers!

© 2016 Wiley-VCH Verlag GmbH & Co. KGaA, Weinheim

Angew. Chem. Int. Ed. **2016**, *55*, 2–17

McDowell, A. C. Nielander, S. Hu, M. R. Shaner, F. Yang, B. S. Brunschwig, N. S. Lewis, *J. Phys. Chem. Lett.* **2015**, *6*, 592–598; c) K. Sun, F. H. Saadi, M. F. Lichterman, W. G. Hale, H.-P. Wang, X. Zhou, N. T. Plymale, S. T. Omelchenko, J.-H. He, K. M. Papadantonakis, B. S. Brunschwig, N. S. Lewis, *Proc. Natl. Acad. Sci. USA* **2015**, *112*, 3612–3617; d) X. Zhou, R. Liu, K. Sun, D. Friedrich, M. T. McDowell, F. Yang, S. T. Omelchenko, F. H. Saadi, A. C. Nielander, S. Yalamanchili, K. M. Papadantonakis, B. S. Brunschwig, N. S. Lewis, *Energy Environ. Sci.* **2015**, *8*, 2644–2649; e) S. Hu, M. R. Shaner, J. A. Beardslee, M. Lichterman, B. S. Brunschwig, N. S. Lewis, *Science* **2014**, *344*, 1005–1009; f) E. Verlage, S. Hu, R. Liu, R. J. R. Jones, K. Sun, C. Xiang, N. S. Lewis, H. A. Atwater, *Energy Environ. Sci.* **2015**, *8*, 3166–3172.

[22] R. C. Rossi, N. S. Lewis, *J. Phys. Chem. B* **2001**, *105*, 12303–12318.

[23] a) A. J. Nozik, *Annu. Rev. Phys. Chem.* **1978**, *29*, 189–222; b) A. Heller, *Acc. Chem. Res.* **1981**, *14*, 154–162; c) N. S. Lewis, *Annu. Rev. Phys. Chem.* **1991**, *42*, 543–580; d) H. Gerischer, *Advances in Electrochemistry and Electrochemical Engineering*, Vol. 1, Interscience, New York, **1961**.

[24] Y. Surendranath, D. K. Bediako, D. G. Nocera, *Proc. Natl. Acad. Sci. USA* **2012**, *109*, 15617–15621.

[25] a) L. Trotochaud, T. J. Mills, S. W. Boettcher, *J. Phys. Chem. Lett.* **2013**, *4*, 931–935; b) J. M. Gregoire, C. Xiang, S. Mitrovic, X. Liu, M. Marcin, E. W. Cornell, J. Fan, J. Jin, *J. Electrochem. Soc.* **2013**, *160*, F337–F342; c) F. Svegl, B. Orel, M. G. Hutchins, K. Kalcher, *J. Electrochem. Soc.* **1996**, *143*, 1532–1539; d) B. Orel, M. Macek, F. Svegl, K. Kalcher, *Thin Solid Films* **1994**, *246*, 131–142.

[26] A. Shinde, D. Guevarra, J. A. Haber, J. Jin, J. M. Gregoire, *J. Mater. Res.* **2014**, 1–9.

[27] A. Heller, D. E. Aspnes, J. D. Porter, T. T. Sheng, R. G. Vadimsky, *J. Phys. Chem.* **1985**, *89*, 4444–4452.

[28] a) Y. K. Chen, K. Sun, H. Audesirk, C. X. Xiang, N. S. Lewis, *Energy Environ. Sci.* **2015**, *8*, 1736–1747; b) E. Kemppainen, A. Bodin, B. Sebok, T. Pedersen, B. Seger, B. Mei, D. Bae, P. C. K. Vesborg, J. Halme, O. Hansen, P. D. Lund, I. Chorkendorff, *Energy Environ. Sci.* **2015**, *8*, 2991–2999.

[29] A. J. Bard, L. R. Faulkner, *Electrochemical Methods, Fundamentals and Applications, 2nd ed.*, Wiley, New York, **2000**.

[30] C. C. L. McCrory, S. Jung, I. M. Ferrer, S. M. Chatman, J. C. Peters, T. F. Jaramillo, *J. Am. Chem. Soc.* **2015**, *137*, 4347–4357.

[31] a) M. A. Modestino, K. A. Walczak, A. Berger, C. M. Evans, S. Haussener, C. Koval, J. S. Newman, J. W. Ager, R. A. Segalman, *Energy Environ. Sci.* **2014**, *7*, 297–301; b) S. M. H. Hashemi, M. A. Modestino, D. Psaltis, *Energy Environ. Sci.* **2015**, *8*, 2003–2009.

[32] E. A. Hernández-Pagán, N. M. Vargas-Barbosa, T. H. Wang, Y. X. Zhao, E. S. Smotkin, T. E. Mallouk, *Energy Environ. Sci.* **2012**, *5*, 7582–7589.

[33] D. A. Vermaas, M. Sassenburg, W. A. Smith, *J. Mater. Chem. A* **2015**, *3*, 19556–19562.

[34] a) K.-T. Jeng, Y.-C. Liu, Y.-F. Leu, Y.-Z. Zeng, J.-C. Chung, T.-Y. Wei, *Int. J. Hydrogen Energy* **2010**, *35*, 10890–10897; b) Y. Leng, G. Chen, A. J. Mendoza, T. B. Tighe, M. A. Hickner, C.-Y. Wang, *J. Am. Chem. Soc.* **2012**, *134*, 9054–9057; c) M. R. Singh, J. C. Stevens, A. Z. Weber, *J. Electrochem. Soc.* **2014**, *161*, E3283–E3296.

[35] a) K. Zeng, D. Zhang, *Prog. Energy Combust. Sci.* **2010**, *36*, 307–326; b) M. Carmo, D. L. Fritz, J. Mergel, D. Stolten, *Int. J. Hydrogen Energy* **2013**, *38*, 4901–4934; c) G. Gahleitner, *Int. J. Hydrogen Energy* **2013**, *38*, 2039–2061; d) A. Ursua, L. M. Gandia, P. Sanchis, *Proc. IEEE* **2012**, *100*, 410–426.

[36] M. I. Gillespie, F. van der Merwe, R. J. Kriek, *J. Power Sources* **2015**, *293*, 228–235.

[37] A. Berger, J. Newman, *J. Electrochem. Soc.* **2014**, *161*, E3328–E3340.

[38] A. Z. Weber, *J. Electrochem. Soc.* **2008**, *155*, B521–B531.

[39] K. D. Kreuer, S. J. Paddison, E. Spohr, M. Schuster, *Chem. Rev.* **2004**, *104*, 4637–4678.

[40] Y. Ma, M. Doyle, T. F. Fuller, M. M. Doeff, L. C. De Jonghe, J. Newman, *J. Electrochem. Soc.* **1995**, *142*, 1859–1868.

[41] C. M. Evans, M. R. Singh, N. A. Lynd, R. A. Segalman, *Macromolecules* **2015**, *48*, 3303–3309.

[42] a) Y. Schneider, M. A. Modestino, B. L. McCulloch, M. L. Hoarfrost, R. W. Hess, R. A. Segalman, *Macromolecules* **2013**, *46*, 1543–1548; b) P. Cotanda, G. Sudre, M. A. Modestino, X. C. Chen, N. P. Balsara, *Macromolecules* **2014**, *47*, 7540–7547; c) A. D. Mohanty, C. Y. Ryu, Y. S. Kim, C. Bae, *Macromolecules* **2015**, *48*, 7085–7095; d) K. M. Meek, S. Sharick, Y. Ye, K. I. Winey, Y. A. Elabd, *Macromolecules* **2015**, *48*, 4850–4862.

[43] a) B. P. Tripathi, V. K. Shahi, *Prog. Polym. Sci.* **2011**, *36*, 945–979; b) H. Zarrin, D. Higgins, Y. Jun, Z. Chen, M. Fowler, *J. Phys. Chem. C* **2011**, *115*, 20774–20781.

[44] A. Roy, M. A. Hickner, X. Yu, Y. Li, T. E. Glass, J. E. McGrath, *J. Polym. Sci. Part B* **2006**, *44*, 2226–2239.

[45] M. B. McDonald, S. Ardo, N. S. Lewis, M. S. Freund, *ChemSusChem* **2014**, *7*, 3021–3027.

[46] K. Sun, R. Liu, Y. Chen, E. Verlage, N. S. Lewis, C. Xiang, *Adv. Energy Materials*, **2016**, 1600379.

[47] a) N. A. Kelly, T. L. Gibson, *Int. J. Hydrogen Energy* **2006**, *31*, 1658–1673; b) H. Dotan, O. Kfir, E. Sharlin, O. Blank, M. Gross, I. Dumchin, G. Ankonina, A. Rothschild, *Nat. Mater.* **2013**, *12*, 158–164; c) B. M. Kayes, H. A. Atwater, N. S. Lewis, *J. Appl. Phys.* **2005**, *97*, 114302.

[48] K. Sivula, *Chimia* **2013**, *67*, 155–161.

[49] J. Brillet, J.-H. Yum, M. Cornuz, T. Hisatomi, R. Solarska, J. Augustynski, M. Graetzel, K. Sivula, *Nat. Photonics* **2012**, *6*, 824–828.

[50] a) R. E. Rocheleau, E. L. Miller, A. Misra, *Energy Fuels* **1998**, *12*, 3–10; b) L. Tong, A. Iwase, A. Nattestad, U. Bach, M. Weidelener, G. Gotz, A. Mishra, P. Bauerle, R. Amal, G. G. Wallace, A. J. Mozer, *Energy Environ. Sci.* **2012**, *5*, 9472–9475.

[51] J. Newman, *J. Electrochem. Soc.* **2013**, *160*, F309–F311.

[52] J. J. Turner, *Nat. Mater.* **2008**, *7*, 770–771.

[53] M. D. Kelzenberg, S. W. Boettcher, J. A. Petykiewicz, D. B. Turner-Evans, M. C. Putnam, E. L. Warren, J. M. Spurgeon, R. M. Briggs, N. S. Lewis, H. A. Atwater, *Nat. Mater.* **2010**, *9*, 239–244.

[54] C. Xiang, A. C. Meng, N. S. Lewis, *Proc. Natl. Acad. Sci. USA* **2012**, *109*, 15622–15627.

[55] M. R. Shaner, K. T. Fountaine, S. Ardo, R. H. Coridan, H. A. Atwater, N. S. Lewis, *Energy Environ. Sci.* **2014**, *7*, 779–790.

[56] a) M. C. Putnam, S. W. Boettcher, M. D. Kelzenberg, D. B. Turner-Evans, J. M. Spurgeon, E. L. Warren, R. M. Briggs, N. S. Lewis, H. A. Atwater, *Energy Environ. Sci.* **2010**, *3*, 1037; b) J. Wallentin, N. Anttu, D. Asoli, M. Huffman, I. Aberg, M. H. Magnusson, G. Siefer, P. Fuss-Kailuweit, F. Dimroth, B. Witzigmann, H. Q. Xu, L. Samuelson, K. Deppert, M. T. Borgstrom, *Science* **2013**, *339*, 1057–1060; c) M. Yao, N. Huang, S. Cong, C. Y. Chi, M. A. Seyedi, Y. T. Lin, Y. Cao, M. L. Povinelli, P. D. Dapkus, C. Zhou, *Nano Lett.* **2014**, *14*, 3293–3303; d) Z. Fan, H. Razavi, J. W. Do, A. Moriwaki, O. Ergen, Y. L. Chueh, P. W. Leu, J. C. Ho, T. Takahashi, L. A. Reichertz, S. Neale, K. Yu, M. Wu, J. W. Ager, A. Javey, *Nat. Mater.* **2009**, *8*, 648–653.

[57] a) N. C. Strandwitz, D. B. Turner-Evans, A. C. Tamboli, C. T. Chen, H. A. Atwater, N. S. Lewis, *Adv. Energy Mater.* **2012**, *2*, 1109–1116; b) C. T. Chen, D. B. Turner-Evans, H. Emmer, S. Aloni, H. A. Atwater, *IEEE Photovoltaic Spec. Conf.* **2013**, 3397–3401; c) A. C. Tamboli, M. Malhotra, G. M. Kimball, D. B. Turner-Evans, H. A. Atwater, *Appl. Phys. Lett.* **2010**, *97*, 221914.

Angew. Chem. Int. Ed. **2016**, *55*, 2–17

© 2016 Wiley-VCH Verlag GmbH & Co. KGaA, Weinheim

www.angewandte.org

These are not the final page numbers!

[58] X. Wang, K.-Q. Peng, Y. Hu, F.-Q. Zhang, B. Hu, L. Li, M. Wang, X.-M. Meng, S.-T. Lee, *Nano Lett.* **2014**, *14*, 18–23.

[59] D. M. Fabian, S. Hu, N. Singh, F. A. Houle, T. Hisatomi, K. Domen, F. E. Osterloh, S. Ardo, *Energy Environ. Sci.* **2015**, *8*, 2825–2850.

[60] Z. G. Zou, J. H. Ye, K. Sayama, H. Arakawa, *Nature* **2001**, *414*, 625–627.

[61] X. C. Wang, K. Maeda, Y. Lee, K. Domen, *Chem. Phys. Lett.* **2008**, *457*, 134–136.

[62] K. Maeda, K. Teramura, K. Domen, *J. Catal.* **2008**, *254*, 198–204.

[63] L. B. Liao, Q. H. Zhang, Z. H. Su, Z. Z. Zhao, Y. N. Wang, Y. Li, X. X. Lu, D. G. Wei, G. Y. Feng, Q. K. Yu, X. J. Cai, J. M. Zhao, Z. F. Ren, H. Fang, F. Robles-Hernandez, S. Baldelli, J. M. Bao, *Nat. Nanotechnol.* **2014**, *9*, 69–73.

[64] J. Liu, Y. Liu, N. Y. Liu, Y. Z. Han, X. Zhang, H. Huang, Y. Lifshitz, S. T. Lee, J. Zhong, Z. H. Kang, *Science* **2015**, *347*, 970–974.

[65] Y. Sasaki, H. Nemoto, K. Saito, A. Kudo, *J. Phys. Chem. C* **2009**, *113*, 17536–17542.

[66] T. F. Yeh, C. Y. Teng, S. J. Chen, H. S. Teng, *Adv. Mater.* **2014**, *26*, 3297–3303.

[67] K. Maeda, M. Higashi, D. L. Lu, R. Abe, K. Domen, *J. Am. Chem. Soc.* **2010**, *132*, 5858–5868.

[68] W. Y. Wang, J. Chen, C. Li, W. M. Tian, *Nat. Commun.* **2014**, *5*, 4647.

[69] Y. Sasaki, H. Kato, A. Kudo, *J. Am. Chem. Soc.* **2013**, *135*, 5441–5449.

[70] K. Maeda, K. Domen, *J. Phys. Chem. Lett.* **2010**, *1*, 2655–2661.

[71] A. Agiral, H. S. Soo, H. Frei, *Chem. Mater.* **2013**, *25*, 2264–2273.

[72] a) M. A. Modestino, S. Haussener, *Annu. Rev. Chem. Biomol. Eng.* **2015**, *6*, 13–34; b) J. Rongé, T. Bosserez, L. Huguenin, M. Dumortier, S. Haussener, J. A. Martens, *Oil Gas Sci. Technol.* **2015**, *70*, 877–889.

[73] J. M. Spurgeon, N. S. Lewis, *Energy Environ. Sci.* **2011**, *4*, 2993–2998.

[74] a) J. M. Spurgeon, M. G. Walter, J. Zhou, P. A. Kohl, N. S. Lewis, *Energy Environ. Sci.* **2011**, *4*, 1772–1780; b) M. R. Shaner, J. R. McKone, H. B. Gray, N. S. Lewis, *Energy Environ. Sci.* **2015**, *8*, 2886–2901.

[75] a) M. A. Modestino, D. K. Paul, S. Dishari, S. A. Petrina, F. I. Allen, M. A. Hickner, K. Karan, R. A. Segalman, A. Z. Weber, *Macromolecules* **2013**, *46*, 867–873; b) M. A. Modestino, A. Kusoglu, A. Hexemer, A. Z. Weber, R. A. Segalman, *Macromolecules* **2012**, *45*, 4681–4688; c) S. A. Eastman, S. Kim, K. A. Page, B. W. Rowe, S. Kang, C. L. Soles, K. G. Yager, *Macromolecules* **2012**, *45*, 7920–7930; d) M. Bass, A. Berman, A. Singh, O. Konovalov, V. Freger, *Macromolecules* **2011**, *44*, 2893–2899; e) D. K. Paul, A. Fraser, K. Karan, *Electrochem. Commun.* **2011**, *13*, 774–777; f) A. Kusoglu, D. Kushner, D. K. Paul, K. Karan, M. A. Hickner, A. Z. Weber, *Adv. Funct. Mater.* **2014**, *24*, 4763–4774; g) F. I. Allen, L. R. Comoli, A. Kusoglu, M. A. Modestino, A. M. Minor, A. Z. Weber, *ACS Macro Lett.* **2015**, *4*, 1–5.

[76] M. A. Modestino, M. Dumortier, M. Hashemi, S. Haussener, C. Moser, D. Psaltis, *Lab Chip* **2015**, *15*, 2287–2296.

[77] S. M. Sze, *Physics of Semiconductor Devices*, 3rd ed., Wiley, New York, **1981**.

[78] V. M. Aroutiounian, V. M. Arakelyan, G. E. Shahnazaryan, *Sol. Energy* **2005**, *78*, 581–592.

[79] E. L. Warren, H. A. Atwater, N. S. Lewis, *J. Phys. Chem. C* **2014**, *118*, 747–759.

■■■■
↖↗ These are not the final page numbers!

www.angewandte.org

© 2016 Wiley-VCH Verlag GmbH & Co. KGaA, Weinheim
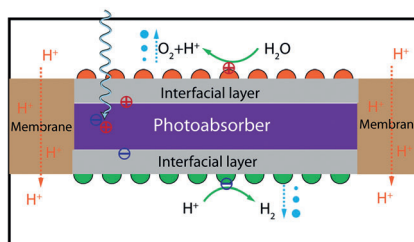
Angew. Chem. Int. Ed. **2016**, *55*, 2–17

Reviews

Solar-Driven Water Splitting

C. Xiang,* A. Z. Weber,* S. Ardo,
A. Berger, Y. Chen, R. Coridan,
K. T. Fountaine, S. Haussener, S. Hu,
R. Liu, N. S. Lewis, M. A. Modestino,
M. M. Shaner, M. R. Singh, J. C. Stevens,
K. Sun, K. Walczak ———— ▮▮▮▮–▮▮▮▮

Modeling, Simulation, and
Implementation of Solar-Driven Water-
Splitting Devices

Catching the sun: Significant advances have been made in recent years on the modeling- and simulation-guided development of integrated solar-driven water-splitting devices. Multidimensional multiphysics models have provided design guidelines for semiconductors, electro-catalysts, as well as liquid and membrane electrolytes. This Review discusses the guiding principles and key findings of these activities.